Electronic Supplementary Material (ESI) for ChemComm.

Formation of a Stable Radical by Oxidation of a Tetraorganoborate

Holger Braunschweig,*[a] Ivo Krummenacher,[a] Lisa Mailänder,[a] Leanne Pentecost[b] and Alfredo Vargas[b]

[a]Institut für Anorganische Chemie, Universität Würzburg, Am Hubland, 97074 Würzburg, Germany.

[b]Department of Chemistry, School of Life Sciences, University of Sussex, Brighton BN1 9QJ, Sussex (UK).

Contents

MATERIALS AND METHODS

All syntheses were carried out with standard Schlenk and glovebox techniques under an argon atmosphere. Solvents were dried by distillation from suitable desiccants (benzene (K) and hexane (Na/K alloy)) under argon and were stored over molecular sieves. Spiroborate $Li[B(C_4Ph_4)_2]$ (**2**) was synthesised following a literature protocol.[1] Ferrocenium hexafluorophosphate was purchased from commercial sources. UV-vis absorption spectra were recorded on a JASCO V-660 UV-vis spectrometer. Elemental analyses were obtained from an Elementar Vario MICRO cube instrument. ESR measurements at X-band (9.4 GHz) were carried out using a Bruker ELEXSYS E580 ESR spectrometer. The spectral simulations were performed using MATLAB 8.3 and the EasySpin 4.5.5 toolbox.[2]

SYNTHESIS OF SPIRO RADICAL **3**

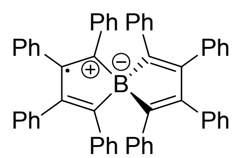

To a solution of the spiroborate lithium salt **2** (30.0 mg, 31.5 μmol) in benzene (3 mL) ferrocenium hexafluorophosphate (10.4 mg, 31.5 μmol) was added at rt. Upon addition, a colour change from yellow over brown to dark green was observed. After stirring the reaction mixture for 20 h at rt, the formed lithium hexafluorophosphate was let to settle and the supernatant solution was separated. After removal of all volatile components under vacuum, the solid residue was washed with hexane until the washings remained colourless. The green raw product was recrystallised from a solution of benzene and diffusion of hexane into the solution at rt. Compound **3** was obtained as a red crystalline solid (18.2 mg, 25.3 μmol, 80%). ^{1}H and ^{11}B NMR: silent; UV-vis (benzene): $\lambda(\varepsilon)_{max}$ = 329 nm (24894 L mol^{-1} cm^{-1}), 352 nm (22919 L mol^{-1} cm^{-1}), 463 nm (12967 L mol^{-1} cm^{-1}), 572 nm (2442 L mol^{-1} cm^{-1}), 604 nm (2307 L mol^{-1} cm^{-1}), ~700.0 nm (~750 L mol^{-1} cm^{-1}); Anal. calc. (%) for $C_{56}H_{40}B$: C 92.94, H 5.57; f.: C 92.41, H 5.82.

CYCLIC VOLTAMMOGRAM OF SPIROBORATE SALT **2**

Cyclic voltammetry experiments were performed using a Gamry Instruments Reference 600 potentiostat. A standard three-electrode cell configuration was employed using a platinum disk working electrode, a platinum wire counter electrode, and a silver wire, separated by a *Vycor* tip, serving as the reference electrode. The potential is referenced to the ferrocene/ferrocenium redox couple ($Fc^{+/0}$) by using ferrocene as an internal standard. Tetra-*n*-butylammonium hexafluorophosphate ([*n*-Bu_4N][PF_6]) was employed as the supporting electrolyte. Compensation for resistive losses (*iR* drop) was employed for the measurement.

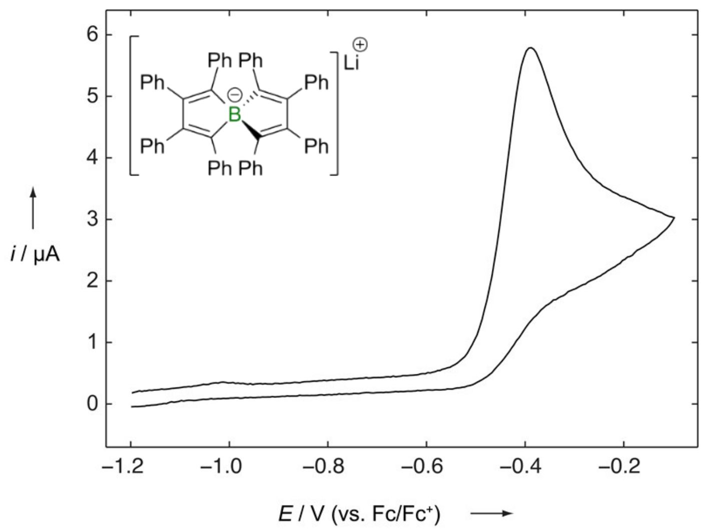

Figure S1. Experimental cyclic voltammogram of spiroborate salt **2** measured in thf/0.1 M [nBu_4N][PF_6] at a scan rate of 250 mV/s. Formal potential: E_{pa} = –0.35 V.

UV-VIS SPECTRUM OF **3**

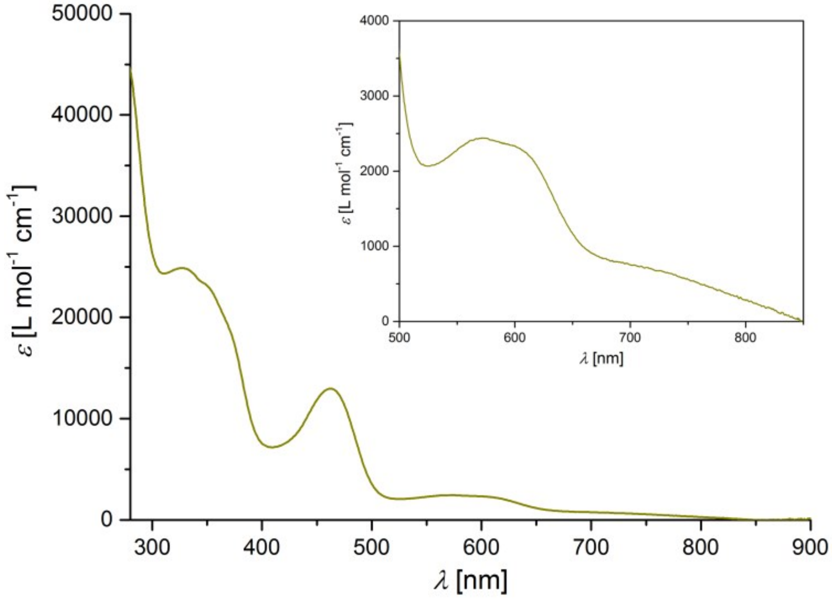

***Figure S2*.** UV-vis spectrum of **3** measured in benzene solution (magnified view in the inset).

X-RAY CRYSTALLOGRAPHIC ANALYSIS OF **3**

The crystal data of **3** were collected on a BRUKER X8-APEX II diffractometer with a CCD area detector and graphite monochromated $Mo_{K\alpha}$ radiation. The structure was solved using intrinsic phasing method (SHELXT), refined with the SHELXL program[3] and expanded using Fourier techniques. All non-hydrogen atoms were refined anisotropically. Hydrogen atoms were included in structure factor calculations. All hydrogen atoms were assigned to idealised geometric positions.

Crystal data for **3**: $C_{56}H_{40}B$, M_r = 723.69, red block, 0.18×0.15×0.08 mm^3, monoclinic space group *P*21/*c*, a = 14.436(8) Å, b = 9.801(3) Å, c = 28.668(4) Å, β = 100.42(3)°, V = 3989(3) Å^3, Z = 4, ρ_{calcd} = 1.205 g·cm^{-3}, μ = 0.068 mm^{-1}, $F(000)$ = 1524, T = 100(2) K, R_1 = 0.1292, wR^2 = 0.2068, 8104 independent reflections [2θ≤52.746°] and 514 parameters.

Crystallographic data have been deposited with the Cambridge Crystallographic Data Center as supplementary publication no. CCDC-1469228. These data can be obtained free of charge from The Cambridge Crystallographic Data Centre *via* www.ccdc.cam.ac.uk/data_request/cif.

Table S1. Bond length and geometric parameters of spiro radical **3** in comparison to the structurally related spiro borate **2**.[1]

Compound	**3**	**2**[1]
Bond length [Å]		
B1–C1	1.503(4)	1.627(2)
B1–C4	1.590(4)	1.637(2)
B1–C5	1.562(5)	1.623(2)
B1–C8	1.489(4)	1.635(2)
C1–C2	1.387(4)	1.368(2)
C2–C3	1.426(4)	1.481(2)
C3–C4	1.439(4)	1.365(2)
C5–C6	1.443(4)	1.363(2)
C6–C7	1.438(5)	1.480(2)
C7–C8	1.396(4)	1.365(2)
Bond angle [°]		
C1–B1–C4	102.7(2)	100.1(2)
C1–B1–C5	117.6(2)	115.3(2)
C1–B1–C8	121.2(2)	112.2(2)
C4–B1–C5	96.4(2)	116.6(2)
C4–B1–C8	113.1(2)	114.3(2)
C5–B1–C8	103.3(2)	99.1(2)
B1–C1–C2	110.0(2)	107.9(2)
C1–C2–C3	111.0(2)	112.0(2)
C2–C3–C4	109.9(2)	111.8(2)
C3–C4–B1	105.6(2)	108.0(2)
B1–C5–C6	105.9(2)	109.2(2)
C5–C6–C7	109.4(2)	111.4(2)
C6–C7–C8	109.9(2)	111.5(2)
C7–C8–B1	110.0(2)	108.6(2)
Torsion angle of BC_4 planes [°]		
	79.0(1)	89.7

DFT CALCULATIONS

Energy minimisation and excitation calculations were conducted within the Kohn-Sham Density Functional Theory (DFT) and so-called Time Dependent Density Functional Theory (TD-DFT)[4-5] at the M062X/6-311G*[6-12] level using the Gaussian09[13] program. To obtain the singlet state, spin-restricted calculations were performed constraining the projection of the total electronic spin along a reference axis to zero. Frequency calculations were conducted to determine if each stationary point corresponds to a minimum. The Wiberg bond indices (WBI)[14] and so-called natural charges were determined in Natural Bond Orbital (NBO)[15-16] basis. The Jmol[17] program was used for visualisation purposes. Excitation calculations were carried out on the gas phase optimized structures within the Time Dependent Density Functional Theory (TD-DFT), absorption spectra were simulated by convoluting the oscillator strengths with Gaussian functions taking the half-bandwidths equal to 4000 cm^{-1} using the SWizard program.[18]

Geometries

Table S2. Comparison of experimental (crystalline) and computational (gas phase) geometries of the neutral radical species.

Parameter	Crystal	M062X
R(B1-C1)	1.488	1.612
R(B1-C4)	1.562	1.614
R(B1-C5)	1.589	1.603
R(B1-C8)	1.503	1.639
A(C1-B1-C4)	103.3	99.18
A(C1-B1-C8)	121.3	104.34
A(C4-B1-C5)	96.4	118.27
A(C5-B1-C8)	102.7	100.11
D(C5-B1-C4-C3)	92.3	142.74
D(C5-B1-C1-C2)	256.3	214.10
D(C4-B1-C5-C6)	95.3	124.26
D(C4-B1-C8-C7)	249.5	231.33

Table S3. Comparison of experimental (crystalline) and computational (gas phase) geometries of the anion species in the singlet state.

Parameter	Crystal	M062X
R(B1-C1)	1.62	1.610
R(B1-C4)	1.63	1.643
R(B1-C5)	1.64	1.618
R(B1-C8)	1.63	1.625
A(C1-B1-C4)	99.1	99.16
A(C1-B1-C8)	115.3	119.92
A(C4-B1-C5)	114.3	105.77
A(C5-B1-C8)	100.1	100.04
D(C5-B1-C4-C3)	123.5	132.59
D(C5-B1-C1-C2)	235.4	240.41
D(C4-B1-C5-C6)	117.5	99.57
D(C4-B1-C8-C7)	242.8	260.25

Frontier Orbitals

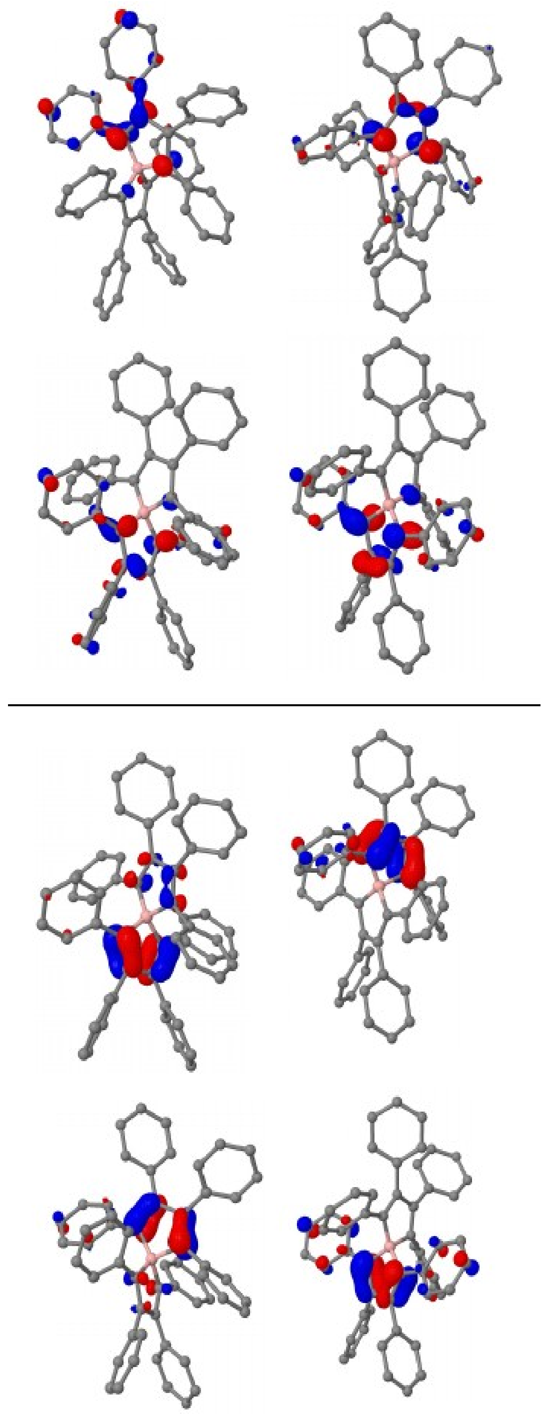

Figure S3. Frontier orbitals of the anion (left) and neutral radical (right) species. Top to bottom: LUMO+1, LUMO, HOMO, HOMO-1.

UV-vis

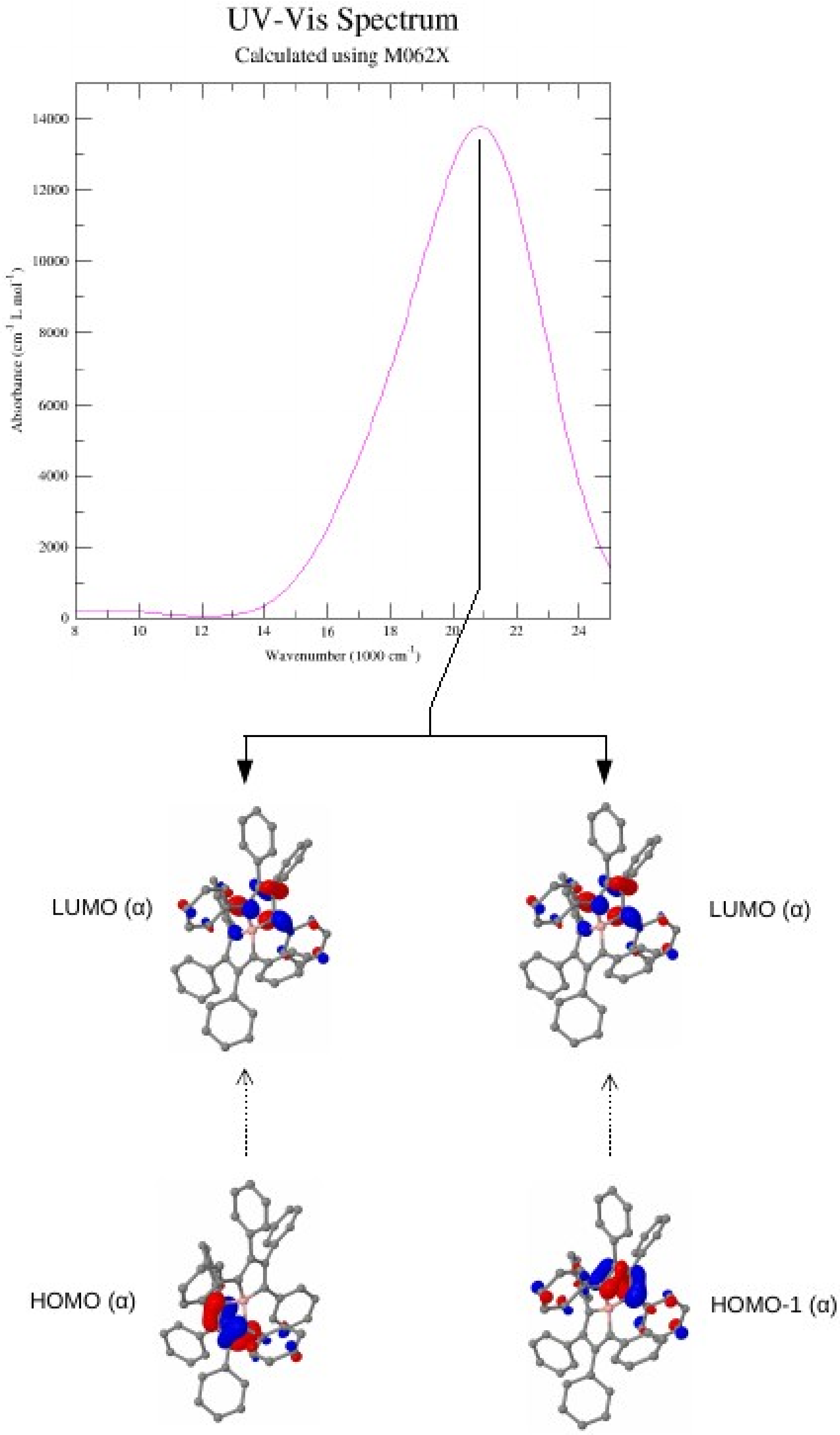

Figure S4. Gas phase UV-vis spectrum calculated using M062X. The two dominant transitions are labelled, with α corresponding to the spin of the electron involved in the transition.

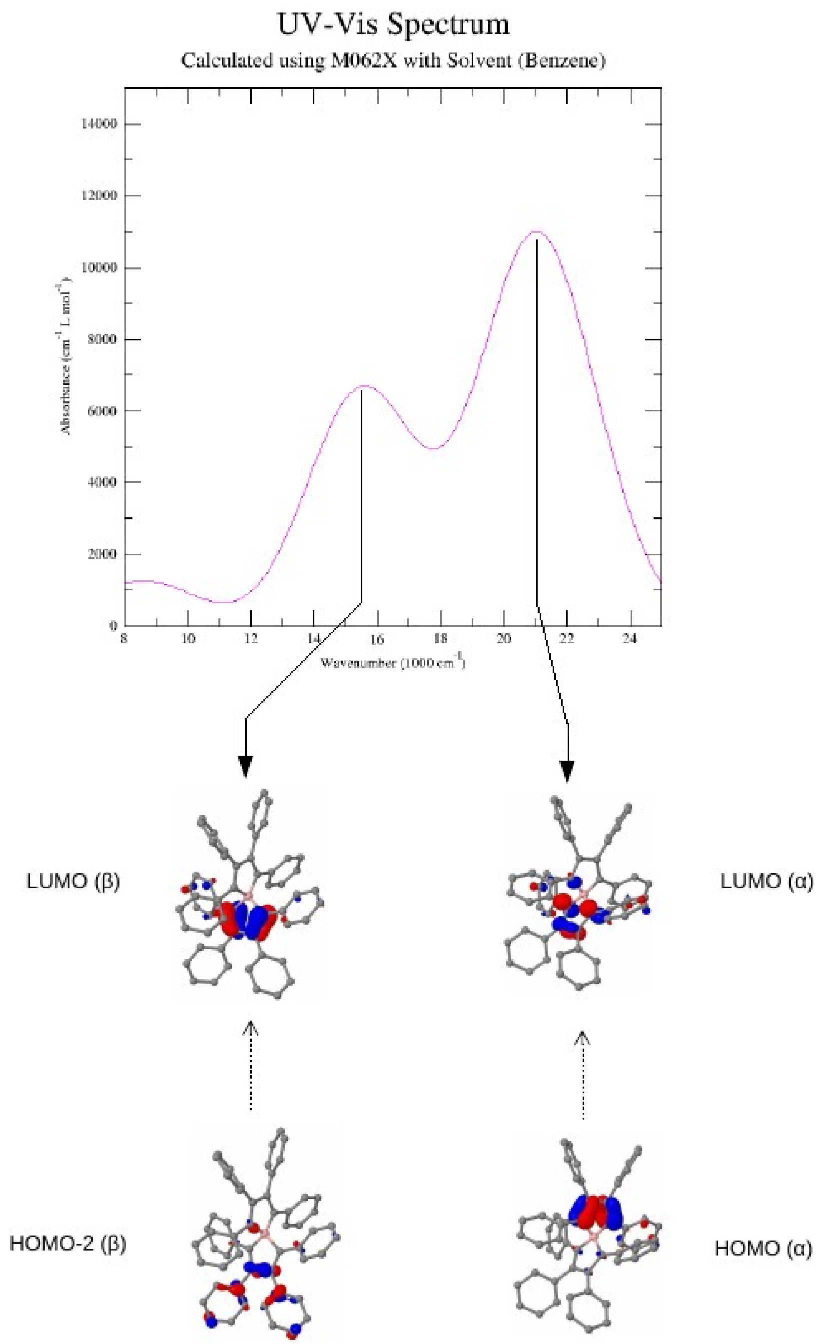

Figure S5. Gas phase UV-vis spectrum calculated using M062X. The two dominant transitions are labelled, with α and β corresponding to the spin of the electron involved in the transition.

Further Structural Investigations

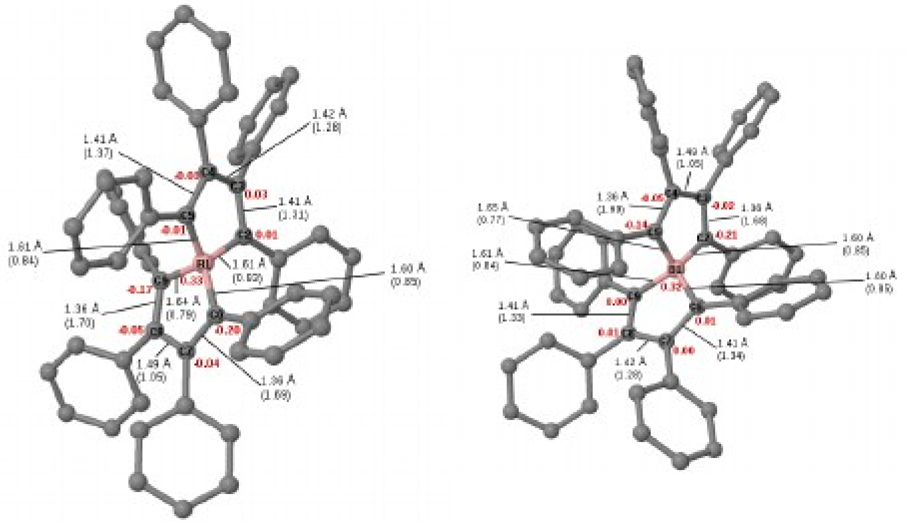

Figure S6. Gas phase (left) and solvent phase (right) structures. Natural charges are in red, and Wiberg Bond Indices are in parentheses.

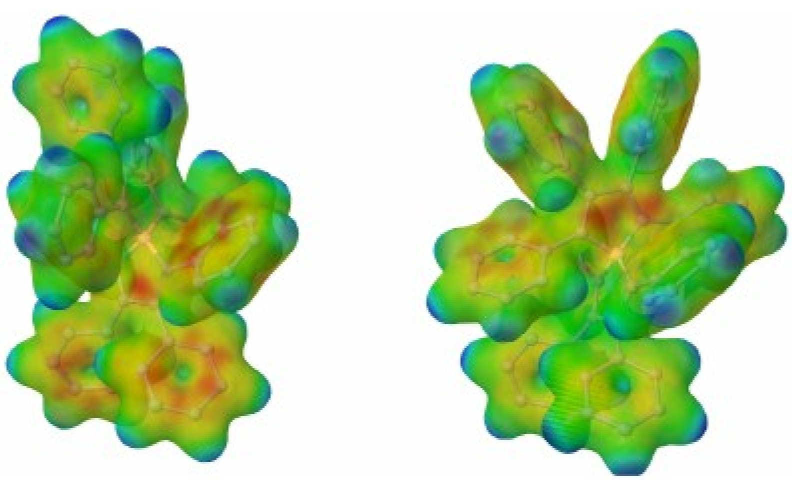

Figure S7. Gas phase (left) and solvent phase (right) MEPs.

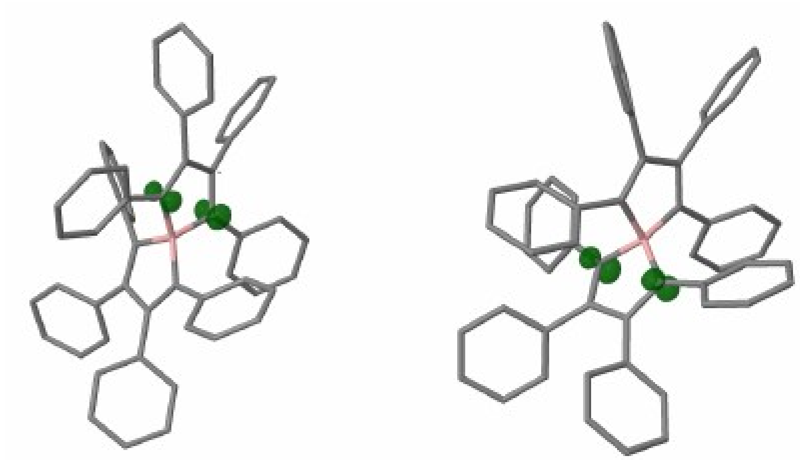

Figure S8. Gas phase (left) and solvent phase (right) spin densities.

***D*$_2$-symmetric Structure**

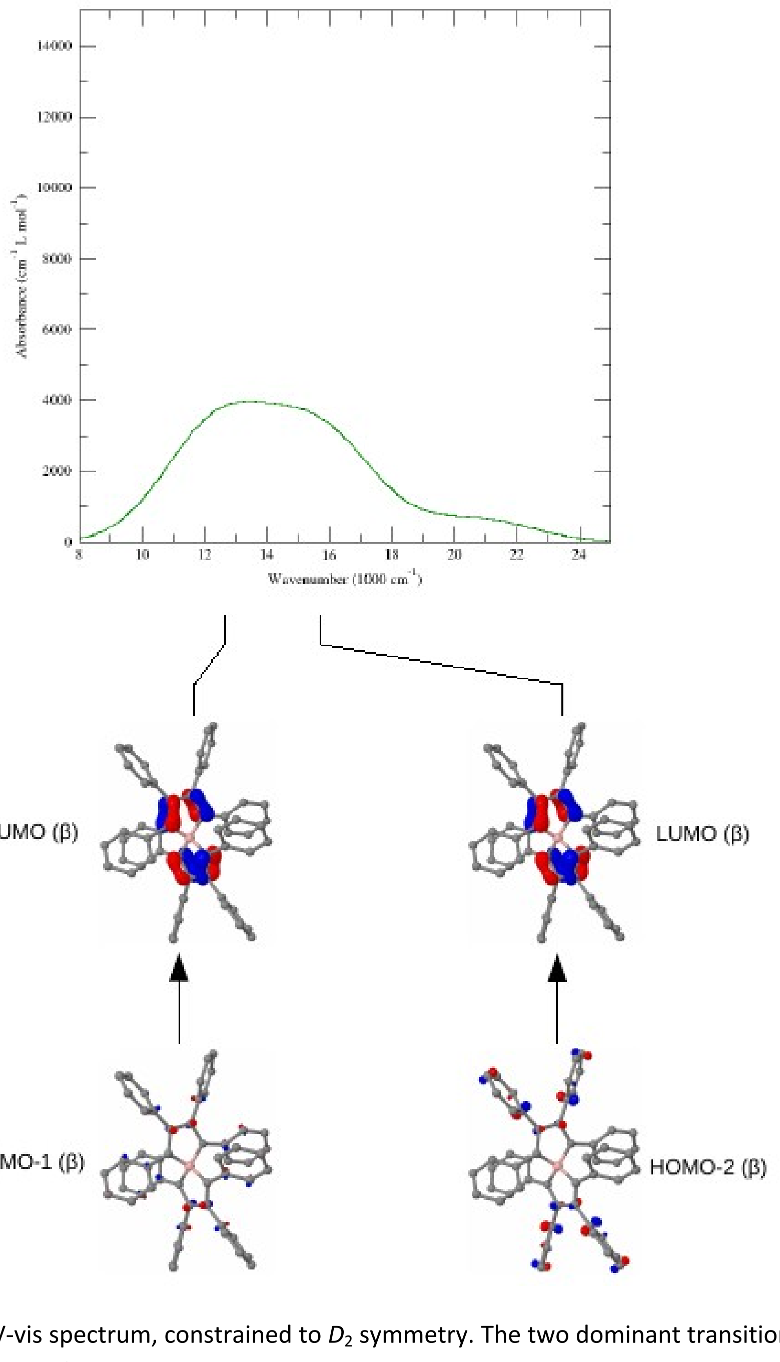

Figure S9. Gas phase UV-vis spectrum, constrained to D_2 symmetry. The two dominant transitions are labelled, with β corresponding to the spin of the electron involved in the transition.

REFERENCES

[1] H. Braunschweig, C. Hörl, F. Hupp, K. Radacki and J. Wahler, *Organometallics*, 2012, **31**, 8463-8466.

[2] S. Stoll and A. Schweiger, *J. Magn. Reson.*, 2006, **178**, 42-55.

[3] G. Sheldrick, *Acta Cryst.*, 2008, **A64**, 112–122.

[4] M. E. Casida, C. Jamorski, K. C. Casida and D. R. Salahub, *J. Chem. Phys.*, 1998, **108**, 4439-4449.

[5] R. Bauernschmitt and R. Ahlrichs, *Chem. Phys. Lett.*, 1996, **256**, 454-464.

[6] Y. Zhao and D. G. Truhlar, *Theor. Chem. Acc.*, 2008, **120**, 215-241.

[7] R. Krishnan, J. S. Binkley, R. Seeger and J. A. Pople, *J. Chem. Phys.*, 1980, **72**, 650-654.

[8] A. J. H. Wachters, *J. Chem. Phys.*, 1970, **52**, 1033-1066.

[9] P. J. Hay, *J. Chem. Phys.*, 1977, **66**, 4377-4384.

[10] K. Raghavachari and G. W. Trucks, *J. Chem. Phys.*, 1989, **91**, 1062-1065.

[11] T. Clark, J. Chandrasekhar, G. W. Spitznagel and P. v. R. Schleyer, *J. Comp. Chem.*, 1983, **4**, 294-301.

[12] M. J. Frisch, J. A. Pople and J. S. Binkley, *J. Chem. Phys.*, 1984, **80**, 3265-3269.

[13] M. J. Frisch, G. W. Trucks, H. B. Schlegel, G. E. Scuseria, M. A. Robb, J. R. Cheeseman, G. Scalmani, V. Barone, B. Mennucci, G. A. Petersson, H. Nakatsuji, M. Caricato, X. Li, H. P. Hratchian, A. F. Izmaylov, J. Bloino, G. Zheng, J. L. Sonnenberg, M. Hada, M. Ehara, K. Toyota, R. Fukuda, J. Hasegawa, M. Ishida, T. Nakajima, Y. Honda, O. Kitao, H. Nakai, T. Vreven, J. A. Montgomery, Jr., J. E. Peralta, F. Ogliaro, M. Bearpark, J. J. Heyd, E. Brothers, K. N. Kudin, V. N. Staroverov, T. Keith, R. Kobayashi, J. Normand, K. Raghavachari, A. Rendell, J. C. Burant, S. S. Iyengar, J. Tomasi, M. Cossi, N. Rega, J. M. Millam, M. Klene, J. E. Knox, J. B. Cross, V. Bakken, C. Adamo, J. Jaramillo, R. Gomperts, R. E. Stratmann, O. Yazyev, A. J. Austin, R. Cammi, C. Pomelli, J. W. Ochterski, R. L. Martin, K. Morokuma, V. G. Zakrzewski, G. A. Voth, P. Salvador, J. J. Dannenberg, S. Dapprich, A. D. Daniels, O. Farkas, J. B. Foresman, J. V. Ortiz, J. Cioslowski and D. J. Fox. Gaussian 09, Revision D.01. Gaussian, Inc., Wallingford, CT, 2013.

[14] K. Wiberg, *Tetrahedron*, 1968, **24**, 1083–1096.

[15] F. Weinhold and C. R. Landis, *Valency and Bonding: A Natural Bond Orbital Donor-Acceptor Perspective*, Cambridge University Press, Cambridge, UK, 2005.

[16] A. E. Reed, L. A. Curtiss and F. Weinhold, *Chem. Rev.*, 1988, **88**, 899–926.

[17] Jmol: an open-source Java viewer for chemical structures in 3D, http://www.jmol.org/

[18] S. I. Gorelsky, SWizard program, revision 4.6, http:/www.sg-chem.net.